Constitutive Modeling for Composite Forming Simulation and Development of a Tool for Composite Material Design

<u>Masato Nishi</u>, Tei Hirashima, Sean Wang
JSOL Corporation

Abstract

Many of the existing FE models in macroscopic forming simulation of fiber fabric have neglected out-of-plane bending stiffness, by using membrane elements, as it is very low compared to in-plane stiffness. To consider this, the shell-membrane hybrid model (S-M model) proposed in the author's previous study can capture bending stiffness as a function of the rotation of the mid-surface. However, influence of the transverse shear deformation upon the bending behavior is not able to be described in this model. In this study, in order to simulate the transverse shear deformation robustly, the thick-shell model (TS model) based on Reissner-Mindlin plate theory is applied in forming simulation of carbon fiber fabric. To compare the predictive capability of out-of-plane deformation, especially wrinkling, by the TS model to the conventional S-M model, we identify the material parameters of each model through a series of coupon experiments. In the S-M model, the bending property is derived from 3-point bending tests across yarn and in a 45° direction, regardless of in-plane properties. On the other hand, the transverse shear modulus is derived from 3-point bending tests with the in-plane properties because the bending behavior results from the rotation of the mid-surface and the transverse shear deformation in the TS model. To complete the study, the forming simulations are carried out by these two FE models and verified by means of comparison with the actual experimental deformations. Small wrinkles that are not captured in the S-M model can be captured in the TS model. Furthermore, a software tool for composite forming simulation that JSOL is developing is presented.

1. Introduction

The forming process of carbon fiber reinforced plastic has increased its presence in the industry due to its wide applicability to mass production. Finite element (FE) simulation is effective in optimizing process conditions, and minimizing lead times and design costs. Dominant deformation modes of fabric materials during forming are in-plane shear and out-of-plane bending due to high deformability. In particular, bending behavior affects the onset and formation of wrinkles, which is one of the major forming defects. Therefore accurate description of bending behavior is an important aspect in the accurate prediction of wrinkles.

Many of the existing FE models in macroscopic forming simulation of carbon fiber fabric have neglected bending stiffness, by using membrane elements, as it is very low compared to in-plane stiffness [1-4]. To consider this, some FE models proposed in recent studies can capture bending stiffness as a bending virtual work separately from in-plane deformation [5, 6]. The shell-membrane hybrid model (S-M model) proposed in the author's previous study also deals with bending stiffness as a function of the rotation of the mid-surface [7, 8]. However, influence of transverse shear deformation upon bending behavior is not able to be described by these models.

In order to simulate transverse shear deformation robustly, the thick-shell model (TS model) is applied in forming simulation in this study. The predictive capability of out-of-plane deformation, especially wrinkling, by the TS model is examined by comparing it to the conventional S-M model, in which out-of-plane bending behavior is simulated independently of in-plane behavior and does not consider transverse shear deformation. The starting point of this study is material parameter identification in each model through a series of coupon experiments. In the S-M model, the bending property is derived from 3-point bending tests across yarn and in a 45° direction. On the other hand, the transverse shear modulus is derived from 3-point bending tests with the in-plane properties because the bending behavior results from the rotation of the mid-surface and the transverse shear deformation in the TS model. Furthermore, the non-linear bending behavior is described by adjusting the in-plane compressive property to be asymmetric to the tensile property. To complete the study, forming simulations are carried out using these two FE models and verified by means of comparison with the actual experimental deformations. Then we evaluate the prediction capability of bending behavior in each model. Small wrinkles that are not captured in the S-M model can be captured in the TS model. Finally, development of a tool for composite material design that JSOL is developing is introduced.

2. Constitutive modeling

Figure 1 shows the constitutive modeling of the S-M model. In-plane properties are described by the membrane element and the bending stiffness is represented by a set of elements which consist of two shell elements with the membrane element in between. It is assumed that the out-of-plane moment is decoupled from the in-plane stress.
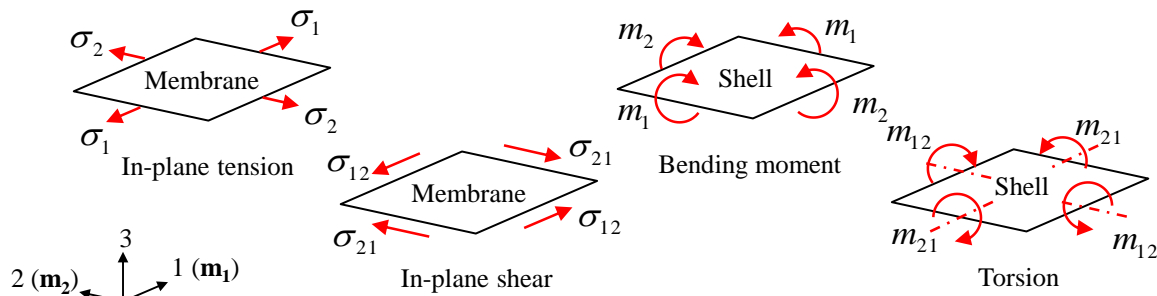

Figure 1: Constitutive modeling of S-M model

*MAT_REINFORCED_THERMOPLASTIC (249) is introduced into the membrane element to describe the in-plane behaviors. This is an anisotropic hyperelastic model which independently calculates tension in the yarn directions and in-plane shear for simulating and considers fiber reorientation under the large shear deformation. Stresses due to elongation of the individual fibers families are then computed as sum:

$$\boldsymbol{\sigma} = \sum_{i=1}^{n} \frac{1}{J} \cdot f(\varepsilon_i) \cdot \mathbf{F} \cdot \left(\mathbf{m}_i^0 \otimes \mathbf{m}_i^0 \right) \cdot \mathbf{F}^T \tag{1}$$

where $\mathbf{m}_i^0$ is an initial yarn direction, and current configuration is given as $\mathbf{m}_i = \mathbf{F}\mathbf{m}_i^0$. $\mathbf{F}$ and J are the deformation gradient tensor and the Jacobian of the deformation, respectively. f, which is

defined by a load curve, is a function to denote a relationship between stress and strain in yarn direction.

Interaction between neighboring fiber families can be accounted for by:

$$\boldsymbol{\sigma} = \sum_{\substack{i,j \\ i \neq j}} \frac{1}{J} \cdot g(\gamma_{ij}) \cdot \mathbf{F} \cdot (\mathbf{m}_i^0 \otimes \mathbf{m}_j^0) \cdot \mathbf{F}^T \qquad (2)$$

Where function *g* to denote a relationship between in-plane shear stress and in-plane shear strain can be provided as a load curve as well.

By using Kirchhoff-Love's (Euler-Bernoulli) [9] assumption that does not take into account transverse shear deformation, a bending deflection *v(x)* for the 3-point bending boundary condition represented in the S-M model is described as follows.

$$v(x) = \frac{P}{12EI} \cdot x \cdot \left(\frac{3}{4} l^2 - x^2 \right) \qquad (3)$$

where *P* is a load at the center point, *EI* is bending stiffness, and *l* is the length between bearings. In this assumption, the cross section remains normal to the mid-surface under the out-of-plane bending deformation as shown in Figure 2. *MAT_ORTHOTROPIC_ELASTIC (002) is used for the shell element to simulate the differences of the bending stiffness in the yarn direction and the 45° direction.
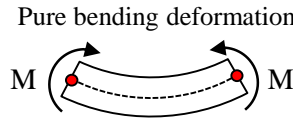

Figure 2: Out-of-plane deformation of S-M model

On the other hand, the TS model based on Reissner-Mindlin plate theory [10] can simulate the transverse shear deformation as shown in Figure 3.
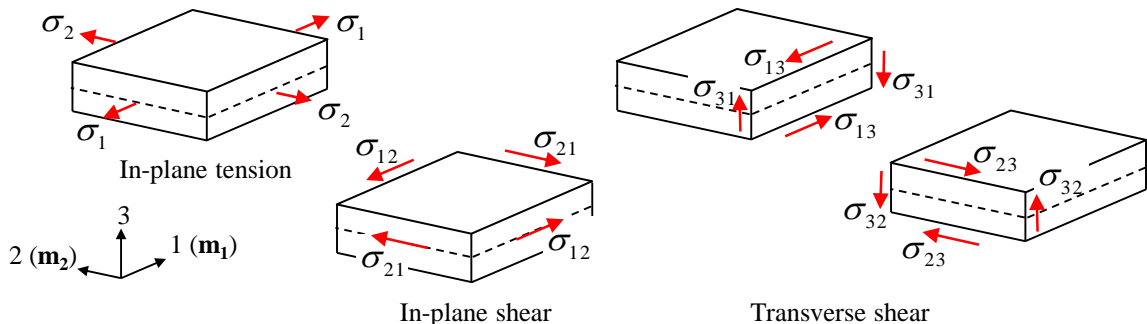

Figure 3: Constitutive modeling of TS model

A bending deflection *v(x)* under a 3-point bending boundary condition in TS model is described by using the Reissner-Mindlin (Timoshenko) assumption. In this assumption, the mid-surface displacement plus rotations are allowed to describe the transverse shear deformation. It is described by Equation (4)

$$v(x) = v_b(x) + v_s(x) = \frac{P}{12EI} \cdot x \cdot \left(\frac{3}{4} l^2 - x^2 \right) + \frac{\alpha \cdot P \cdot x}{2G \cdot A} \tag{4}$$

where $v_b(x)$ and $v_s(x)$ are the deflection due to pure bending deformation and the deflection due to transverse shear deformation, respectively; κ is the shear correction factor and A is the cross section area. Equation (5) shows that the out-of-plane deformation in the TS model represents two deformation modes. One is the pure bending expressed in first term, and the other is the transverse shear deformation expressed in second term, as shown in Figure 4.
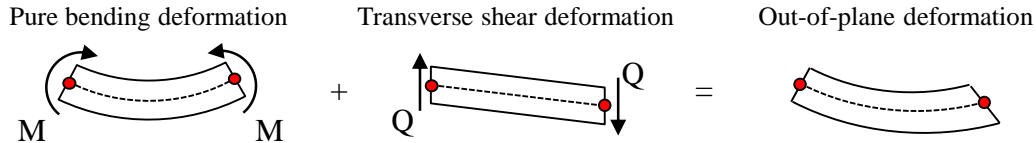

Figure 4: Out-of-plane deformation of TS model

*MAT_REINFORCED_THERMOPLASTIC (249) is also applied to the thick-shell element to deal with a large in-plane shear deformation.

3. Parameter identification

In this section, the identification processes for material parameters in the S-M model and the TS model will be discussed. A plain-weave carbon fabric (T300-3K, Toray) is used in this study. Each parameter in each model is identified through a series of coupon tests, uniaxial tension across yarn direction, bias-extension and 3-point bending across yarn direction and in 45° direction, as shown in Figure 5.

Stress–strain relationship *f* in yarn direction is obtained from a uniaxial tension test across yarn direction. The uniaxial tension specimen is rectangular with a free clamping length of 80 mm and a width of 24 mm. During the uniaxial tension test, displacement and force history are recorded. The force is measured by a load cell (max. 10 kN) and the displacement is measured optically by a high-speed camera. The stress–strain relationship is derived from measured local displacement and load history. In the S-M model, a compressive stress–strain relationship is assumed as being symmetric to the tensile property.

In-plane shear stress–shear strain relationship *g* is obtained from a bias-extension test. A bias-extension test is a popular approach to measure the shear property of dry fabrics and prepregs. It is a tensile test performed on a rectangular specimen where the warp and weft yarns are oriented initially 45/-45 to the direction of applied tensile load, as shown in Figure 6 (a). The dimension of the bias-extension test specimen is a free clamping length of 120 mm and a width of 30 mm with a ratio of length to width of 4:1. During the bias-extension test, displacement and force history is recorded. The load is measured by a load cell (max. 50N). If the yarns are considered inextensible and no intra-ply slip occurs within the specimen (correlation with the Pin Jointed Net assumption [11]), shear angle γ_{12} and shear stress σ_{12} are calculated as follows.

$$\gamma_{12} = \frac{\pi}{2} - 2\arccos\left(\frac{H - W + d}{\sqrt{2}(H - W)} \right) \tag{5}$$

$$\sigma_{12}(\gamma_{12}) = \frac{1}{(2H - 3W) \cdot t \cdot \cos\gamma_{12}} \left(\left(\left(\frac{H}{W} - 1\right) \cdot F \cdot \left(\cos\frac{\gamma_{12}}{2} - \sin\frac{\gamma_{12}}{2}\right)\right.\right.$$
$$\left.\left. -W \cdot \sigma_{12}\left(\frac{\gamma_{12}}{2}\right) \cdot \cos\frac{\gamma_{12}}{2} \cdot t \right)\right) \tag{6}$$

where *F* and *d* are the load cell force and the applied displacement of the crosshead of the testing, respectively. *H*, *W* and *t* are the length, width and thickness of specimen. Figure 6 (b) shows the in-plane shear property characterized form the bias-extension test by using Equation (5) and Equation (6).
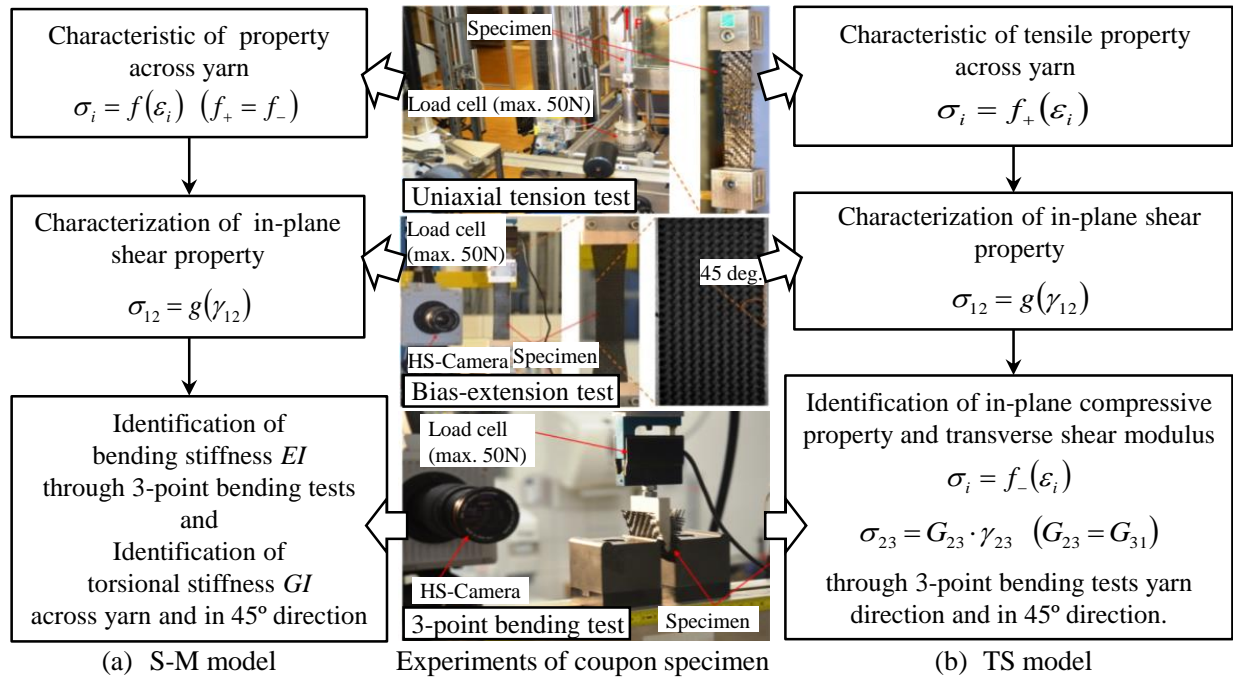

(a) S-M model   Experiments of coupon specimen   (b) TS model

Figure 5: Identification process of material parameters through coupon experiments

(a) Bias-extension specimen before and after testing   (b) Shear stress – shear strain curve
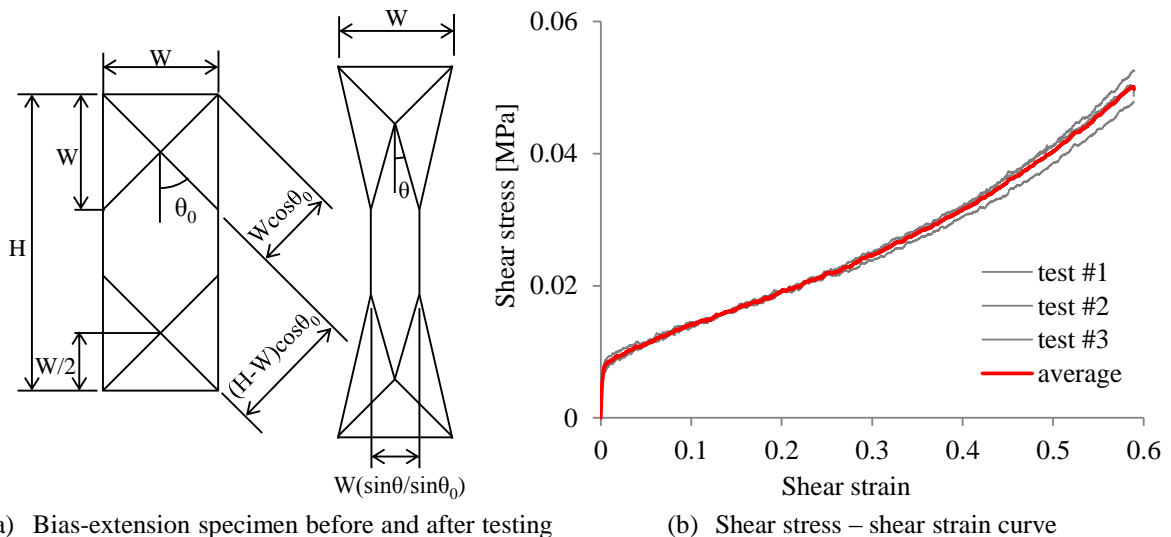
Figure 6: Kinematic of bias-extension test and characterized shear property

Out-of-plane material parameters are identified from 3-point bending tests as shown in Figure 7 (a). The bending specimens are quadratic with a size of 40 mm. During the bending tests, displacement and force histories are recorded. The force is measured by a load cell (max. 50N). The displacement of the center of the specimen is determined by the displacement of the crosshead of the testing machine. By the use of beam theory, bending stiffness EI in the S-M model is derived from measured displacement and force history in yarn direction, and torsion stiffness GI is calculated from the bending test in 45˚ direction as well.

Transverse shear modulus G_{23} ($=G_{31}$) and the compressive property in yarn directions f_- in the TS model are identified by fitting the experimental results of the 3-point bending tests in yarn and 45˚ directions. An optimization tool LS-OPT® is used. The resultant force–displacement curves converged in about 4 iterations using the mean squared error method [12]. The optimized history is shown in Figure 8.
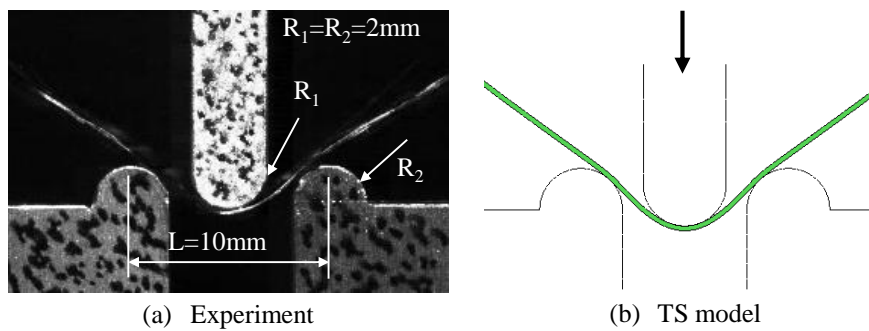

(a) Experiment   (b) TS model

Figure 7: Deformations under 3-point bending along yarn direction

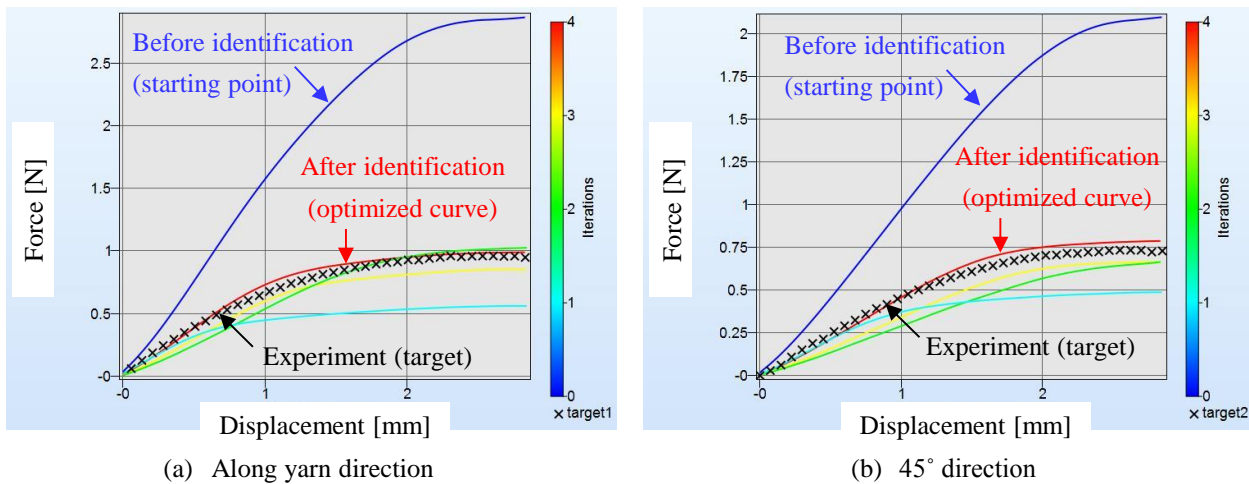(a) Along yarn direction   (b) 45˚ direction

Figure 8: Out-of-plane responses under 3-point bending at various iterations in LS-OPT

The transverse shear modulus G_{23} ($=G_{31}$) in the TS model that has been identified from the 3-point bending tests is very small. It is clear from Equation (4) that the ratio of the transverse shear deflection $v_s(x)$ to the bending deflection $v_b(x)$ increases under the shorter length between bearings. This suggests that the predictable possibility for a small wrinkle, which is difficult to predict in the conventional FE model like the S-M model, increases in the TS model since this accounts for transverse shear deformation.

4. Forming simulation

Forming simulations are performed by using the identified parameters in both the S-M model and the TS model, and compared to the experimental deformations including the wrinkles during the forming process. A schematic figure of the FE model is shown in Figure 9. The blank size is 280 × 280 mm with a thickness of 0.23 mm. It is meshed with 313,600 elements. Upper and lower forming tools are modeled as rigid bodies. The carbon fiber fabric is in tension during the forming process by gripping it at 4 corners. The downward movement of upper tool is 20 mm.
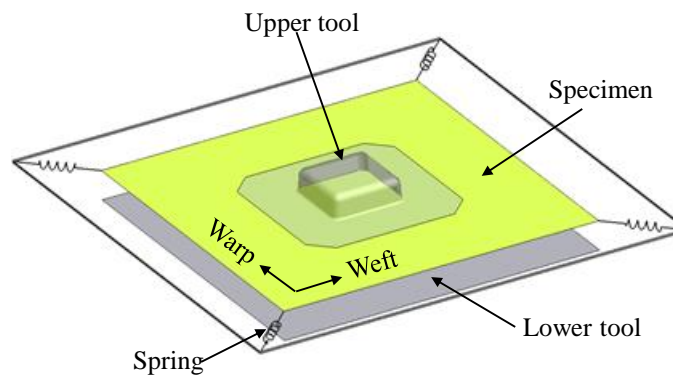

Figure 9: FE model of square tube forming

Figure 10 shows the top view of the deformation of the blank during the forming experiment. Wrinkles are observed around the corners and develop along with the movement of tool. A large and a small wrinkle are observed as shown in Figure 10 (b). In the forming process, it is necessary to undergo in-plane deformation to conform the blank to the tool geometry. A large in-plane shear deformation typically occurs during forming of a carbon fiber fabric since the in-plane shear resistance is very low until the shear locking angle. If the shear deformation reaches the locking angle, out-of-plane wrinkling occurs.
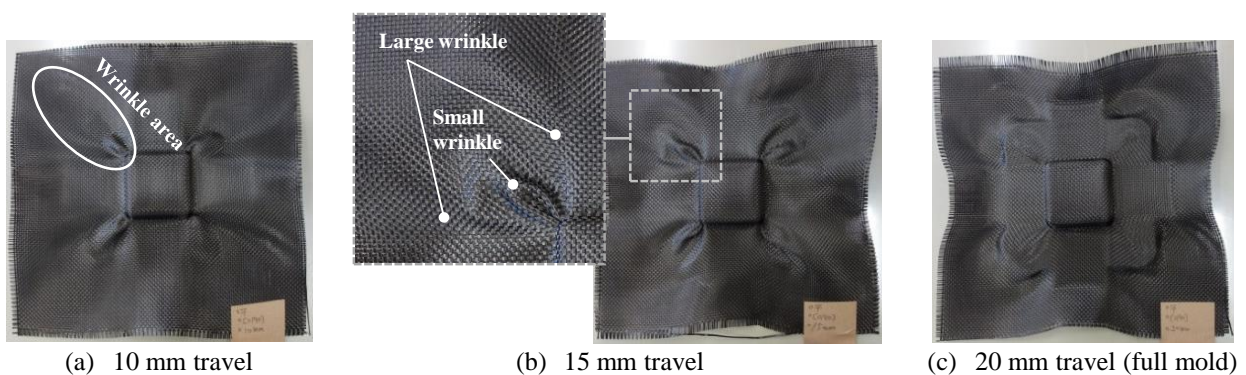

(a)   10 mm travel   (b)   15 mm travel   (c)   20 mm travel (full mold)

Figure 10: Wrinkles observed during forming experiment

Predictive deformations at 15 mm travel, 5 mm remaining closure travel, by both the S-M model and the TS model, are shown in Figure 11. In Figure 11 (a), large wrinkles are actually present around the corners in the S-M model. These were also observed in the forming experiments, but

the experiments showed small wrinkles between the large wrinkles as shown in Figure 10 (b). As expected, small wrinkles are not represented in the S-M model. Figure 11 (b) shows the simulated deformation in the TS model. The small wrinkles that are not captured in the S-M model can be captured in the TS model.
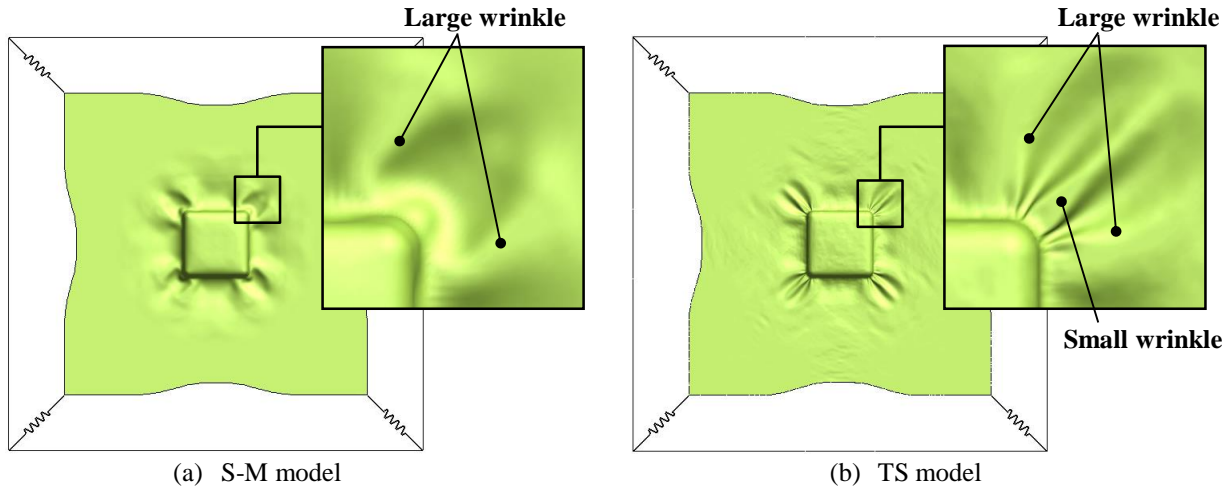

(a) S-M model   (b) TS model

Figure 11: Comparison of wrinkle shapes of S-M model and TS model at 15mm travel

These simulation results demonstrate that when identifying bending stiffness, a conventional model which treats bending independently, like the S-M model, is insufficient to reproduce small wrinkles caused by transverse shear deformation. They also show that the TS model, which considers out-of-plane shear, is an effective approach.

5. Development of a tool for composite forming

Constitutive modelling for composite forming simulation is relatively complex and high effort by users is needed to become familiar with it. Thus, JSOL is developing a software tool for the forming simulation of woven fabrics, non-crimp fabrics unidirectional tapes and pre-pregs (thermoset and thermoplastic).
The following features are planned:
- ➢ Meshing
- ➢ Material characterization
    - ✧ Automatic creation of material model based on experimental results
- ➢ Material database
    - ✧ Standardly included calibrated material models (dry woven fabric, thermoset and thermoplastic prepregs)
- ➢ Model set up
    - ✧ Define lay-up (number of plies, orientation, thickness and contact between layers)
- ➢ Formability analysis
    - ✧ Wrinkle, fiber orientation and plat pattern
- ➢ Mapping
    - ✧ Map data from forming simulation to crash model

The tool helps users to set up the input data and conduct composite forming simulations with LS-DYNA®. Furthermore, because the performance of the final composite part strongly depends

on changes in fiber orientation during the forming process, fiber orientation after the forming process can be mapped to a model for crash simulation.
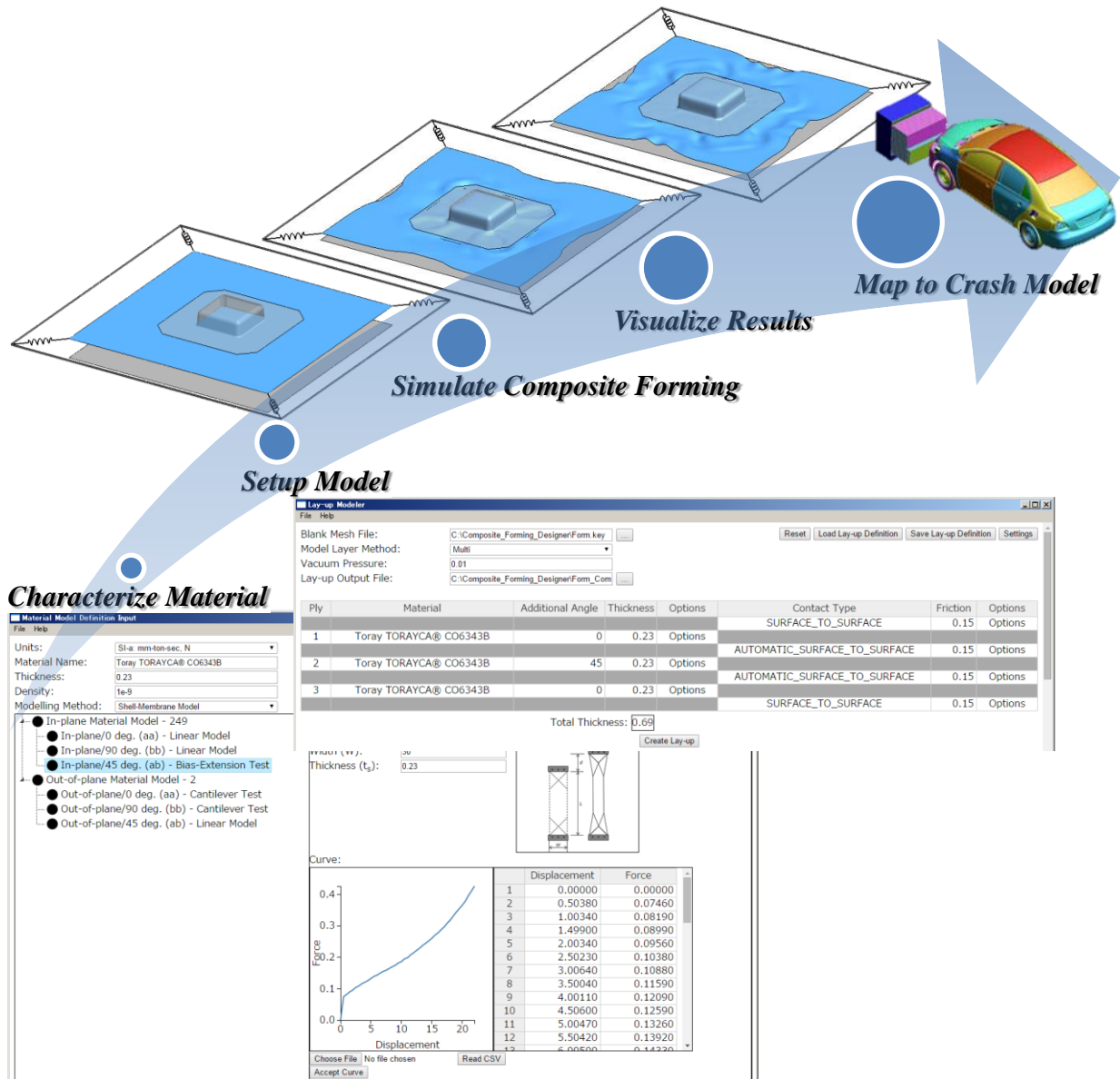

Figure 12: Software tools for composite forming simulation

6. Summary and outlook

The influence of transverse shear deformation upon bending behavior, especially small wrinkling, was numerically examined in this paper. Forming simulations were carried out with two FE models, an S-M model and a TS model, and show that small wrinkles that were not captured in the S-M model were captured in the TS model. It has become clear that the small wrinkles are predominantly caused by transverse shear deformation. Furthermore, a software tool for composite forming simulation that JSOL is developing was presented.

This study presented the prediction capability of wrinkling in the forming simulation of single-layered composite. However, forming multi-layered composites together is a more widespread

process in the industry. In the forming of multi-layered composites, out-of-plane wrinkling occurs due to the combination of intra-ply material deformations and inter-ply slippage. In several papers [13-15], the Stribeck curve that is the Coulomb friction coefficient as a function of the Hersey number has been described to model the intra-ply friction properties between prepregs as a combination of viscous friction and Coulomb friction in parallel. A new contact _LUBRICATION is implemented to capture the slippage behavior between prepregs as shown in Figure 12. Additionally an adhesion in normal direction can be considered as well.
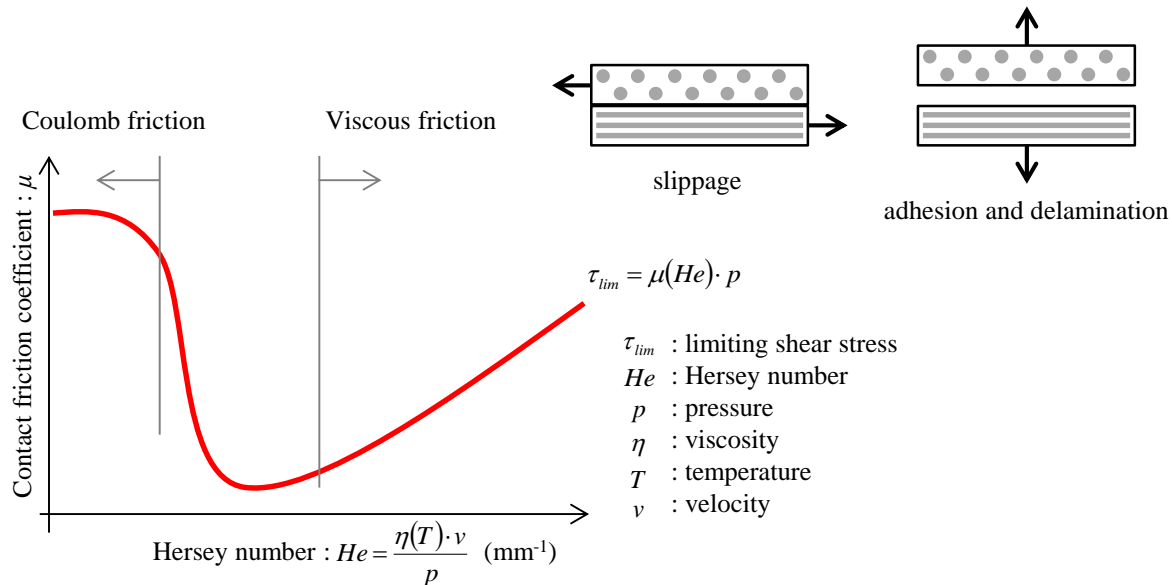

$$\tau_{lim} = \mu(He)\cdot p$$

τ_{lim} : limiting shear stress
He : Hersey number
p : pressure
η : viscosity
T : temperature
v : velocity

Hersey number : $He = \dfrac{\eta(T)\cdot v}{p}$ (mm⁻¹)

*Figure 13: New option, _LUBRICATION, for *CONTACT keyword*

Acknowledgements

References

[1] P. Xue et al., A non-orthogonal constitutive model for characterizing woven composites, Composites Part A, vol.34, pp.183–193, (2003).
[2] A. Willems et al., Forming simulation of a thermoplastic commingled woven textile on a double dome, International Journal of Material Forming, vol.1, pp.965-968, (2008).
[3] R.H.W. ten Thije et al., A multi-layer triangular membrane finite element for the forming simulation of laminated composites, Composites Part A, vol.40, pp.739–753, (2009).
[4] Y. Aimene et al., A hyperelastic approach for composite reinforcement large deformation analysis, Journal of Composite Materials, vol.44, pp.5-26, (2010).
[5] P. Boisse et al., Simulation of wrinkling during textile composite reinforcement forming. Influence of tensile, in-plane shear and bending stiffnesses, Composites Science and Technology, vol.71, pp.683–692, (2011).

[6] S.P. Haanappel et al., Formability analyses of uni-directional and textile reinforced thermoplastics, Composites Part A, vol.56, pp.80-92, (2014).

[7] M. Nishi et al., Textile composite reinforcement forming analysis considering out-of-plane bending stiffness and tension dependent in-plane shear behavior, ECCM16 (2014).

[8] M. Nishi et al., Forming simulation of textile composites using LS-DYNA, 10ᵗʰ European LS-DYNA Conference (2015).

[9] G. Kirchhoff, Über das Gleichgewicht and die Bewegung einer elastischen Scheibe, Journal für reine und angewandte Mathematik, vol.40, pp.51-88, (1850).

[10] R.D. Mindlin, Influence of rotatory inertia and shear on flexural motions of isotropic, elastic plates, Journal of Applied Mechanics, vol.18, pp.31-38, (1951).

[11] W. Lee et al., Bias-extension of woven composite fabrics, International Journal of Material Forming, vol.1, pp. 895-898, (2008).

[12] N. Stander et al., LS-OPT® user's manual, Livermore Software Technology Corporation, (2010).

[13] Y.R. Larberg et al., On the interply friction of different generations of carbon/epoxy prepreg systems, Composites Part A, vol.42, pp.1067-1074, (2011).

[14] Q. Chen et al., Intra/inter-ply shear behaviors of continuous fiber reinforced thermoplastic composites in thermoforming processes, Composite Structures, vol.93, pp.1692-1703, (2011).

[15] P. Wang, et al., Thermoforming simulation of multilayer composites with continuous fibres and thermoplastic matrix, Composites Part B, vol.52, pp.127–136, (2013).